

A mathematical model of liver cell aggregation *in vitro*

J.E.F. Green^{*†} S.L. Waters^{*‡} K.M. Shakesheff[§] H.M. Byrne^{*}

April 2, 2008

Abstract

The behaviour of mammalian cells within three-dimensional structures is an area of intense biological research and underpins the efforts of tissue engineers to regenerate human tissues for clinical applications. In the particular case of hepatocytes (liver cells), the formation of spheroidal multicellular aggregates has been shown to improve cell viability and functionality compared to traditional monolayer culture techniques. We propose a simple mathematical model for the early stages of this aggregation process, when cell clusters form on the surface of the extracellular matrix (ECM) layer on which they are seeded. We focus on interactions between the cells and the viscoelastic ECM substrate. Governing equations for the cells, culture medium and ECM are derived using the principles of mass and momentum balance. The model is then reduced to a system of four partial differential equations, which are investigated analytically and numerically. The model predicts that, provided cells are seeded at a suitable density, aggregates with clearly defined boundaries and a spatially uniform cell density on the interior will form. While the mechanical properties of the ECM do not appear to have a significant effect, strong cell-ECM interactions can inhibit, or possibly prevent, the formation of aggregates. The paper concludes with a discussion of our key findings and suggestions for future work.

Keywords: Cell aggregation, tissue engineering, multiphase model

^{*}Centre for Mathematical Medicine and Biology, School of Mathematical Sciences, University of Nottingham, Nottingham, NG7 2RD, UK.

[†]Corresponding author - email: egreen@mbi.osu.edu. Current address: Mathematical Biosciences Institute, The Ohio State University, Columbus, Ohio, 43210 USA.

[‡]Current address: Oxford Centre for Industrial and Applied Mathematics, Mathematical Institute, 24-29 St Giles', Oxford, OX1 3LB, UK.

[§]Tissue Engineering Group, School of Pharmacy, University of Nottingham, Nottingham, NG7 2RD, UK.

1 Introduction

The liver is the largest, most metabolically complex organ in humans, weighing approximately 1.5 kg, and performing an estimated 500 different functions. Diseases of the liver, including hepatitis and cirrhosis, caused about 46,000 deaths in the USA in 1998 (Centers for Disease Control and Prevention, 2003), and at present there are few successful treatments for such conditions apart from organ transplant. Whilst waiting lists for transplants continue to lengthen, the level of organ donation has remained static (OPTN, 2003; NHS, 2001), so interest is now turning to the development of liver support devices. Passive systems to remove blood toxins accumulated during liver failure (*e.g.* haemodialysis, haemofiltration and plasma exchange) have shown disappointing results in terms of patient survival, and so attention has focused on cell-based liver support devices (Jauregui, 2000). The engineering of liver tissue for such devices, for drug testing and, potentially, for transplantation, has stimulated new interest in understanding the interactions between the cell populations in the liver, various growth factors and the extracellular matrix (ECM).

In vivo, under normal physiological conditions, around 80% of liver tissue is composed of hepatocytes (Mitaka, 1998). These epithelial cells perform most of the liver's important functions (Selden et al., 1999), and hence have received the greatest attention from tissue engineers. Hepatocytes cultured *in vitro* often form a monolayer, have a tendency to de-differentiate (lose their ability to function normally) within hours, and die after a few days (Riccaltón-Banks et al., 2003; Bhandari et al., 1997). Techniques that have been developed to overcome this problem include co-culture with other cell types (such as stellate cells, also found in the liver), culture on polymer scaffolds and the use of growth factors and cytokines (Bhandari et al., 1997). Some of these techniques result in the hepatocytes forming multicellular spheroids. The structure of the spheroids appears to mimic, in some respects, that of liver tissue *in vivo* - for example, channels resembling bile canaliculi are seen (Abu-Absi et al., 2002). Spheroid culture also results in prolonged expression of liver-specific functions (commonly measured by albumin production (Riccaltón-Banks, 2002)) and hepatocyte viability (Richert et al., 2002).

A common procedure for culturing hepatocytes as spheroids involves seeding the freshly isolated cells in culture wells coated with ECM and bathed in a culture medium, which supplies them with nutrients. On suitable substrates, the cells aggregate over a period of approximately one day (Riccaltón-Banks, 2002) (Glicklis et al. (2000) also report clustering

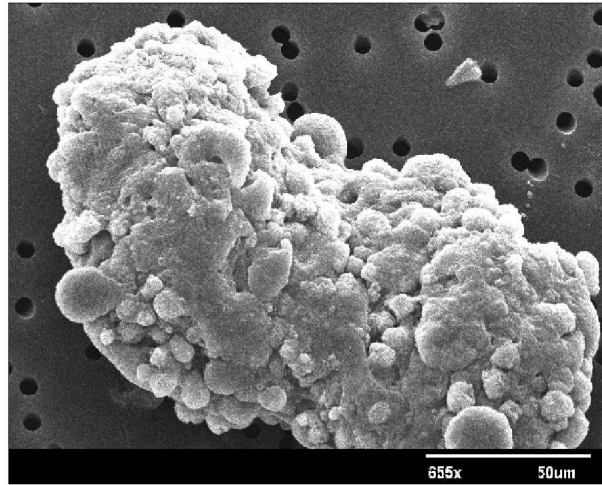


Figure 1: Scanning electron micrograph of a multicellular liver spheroid (courtesy of L. Riccalton-Banks)

over a similar timescale for hepatocytes seeded in alginate scaffolds). These aggregates then detach themselves from the surface of the ECM and reorganise to form multicellular spheroids, the diameter of which is around 100-150 μm (Thomas et al., 2005), as we can see from Fig. 1 (compared to a representative cell diameter of 10-30 μm (Higuchi and Tsukamoto, 2004; Glicklis et al., 2000)). The migration of hepatocytes during the early stages of aggregation is described in detail in Powers and Griffith-Cima (1996). They found that only around 6 % of observed cells exhibited ‘classical single-cell locomotion’, defined as occurring when a cell translates one body length, without contacting another cell. More frequently, direct cell-cell contact caused by membrane extension facilitated the formation of aggregates. Translation of groups of cells was not quantified in their study, although the authors state that many of the cells translated more than one body length following cell-cell contact.

Hepatocytes are anchorage-dependent cells (Bhandari et al., 1997; Selden et al., 1999), and their interactions with the ECM are believed to be of great importance, both *in vivo* (Bedossa and Paradis, 2003) and *in vitro*. Significantly, experiments have shown that the material properties of the ECM affects the morphology of the cells, the likelihood of aggregation, and the ability of the cells to sustain liver specific functions (Moghe et al., 1996; Powers et al., 1997). Tissue engineers employ a wide variety of ECM types; often these are artificial substrates such as tissue culture plastic or polylactic acid; however,

unlike the ECM *in vivo*, such substrates lack specific recognition groups for cells. Matrix proteins such as fibronectin can be employed to modify such surfaces, and provide a more favourable environment for attachment (see Whitaker (2003, Ch. 5)). Another approach is to culture the cells on natural ECM components, such as Matrigel or in a collagen sandwich (Richert et al., 2002). In addition to cell-ECM interactions, cell-cell contacts appear to play a significant role, and studies have shown that spheroid formation is inhibited if the initial cell plating density is too high or too low (Peshwa et al., 1996, 1994). Cell-cell interactions are also important in maintaining the viability and functionality of the hepatocytes (Moghe et al., 1997).

Previous modelling work on this problem appears limited. Glicklis et al. (2004) assumed the diameter of individual liver cell spheroids undergoes logistic growth, and determined the values of the relevant parameters by fitting to experimental data. They then used this solution to determine the rate of albumin production. By contrast, cell aggregation in the slime mould *Dictyostelium discoideum* has been extensively studied by theoreticians. In this organism, when nutrients are scarce, aggregation is stimulated by gradients of a cell-derived chemical (cAMP) (Vasiev and Weijer, 2003). This phenomenon provided the motivation for the development of the best known model for chemotactic cell movement, due to Keller and Segel (1970, 1971). Although chemotaxis is also a potential mechanism for hepatocyte aggregation (see §6), for simplicity we do not explicitly consider chemical signals in this paper. Instead, we base our approach on the ideas of Murray and co-workers (Murray, 1993), who developed continuum models which include the effects of cell interactions with the ECM. They propose a general equation for the evolution of the cell density, in which cell movement involves a combination of random motion, chemotaxis and advection with the ECM. The principles of mass and momentum balance are used to derive equations for the density and deformations of the ECM. Models of this type offer enormous scope for generating many different types of spatial patterns, and have been studied in connection with a wide variety of systems, including limb-bud formation, wound healing and cancer. An alternative approach that has been used to describe the formation of vascular networks *in vitro*, involves coupling a mass conservation equation for the cell density to a Burgers-type equation for the cell velocity (Kowalczyk et al. (2004) and references therein), rather than simply prescribing the cell flux as a function of cell density and ECM displacement as in Murray (1993). The velocity equation also contains

a Keller-Segel type term describing chemotaxis, which is in turned coupled to a reaction diffusion equation for the chemoattractant in the conventional way.

As the review above suggests, there is increasing interest in developing mathematical models which describe interactions between cells and other constituents of their environment, such as extracellular fluid (Breward et al., 2002), ECM (Jackson and Byrne, 2002; Lemon et al., 2006) and other cell populations *e.g.* macrophages (Owen et al., 2004). Multiphase models, in which the different components are treated as distinct phases, represent a natural framework within which to study such systems. The principles of mass and momentum conservation are applied to each phase, and the physical properties of the different phases, and the interaction forces between them, specified by constitutive relations. We use this approach here to study the early stages of liver cell spheroid formation.

The paper is organised as follows: in §2, we derive the governing equations and show how they may be reduced to a system of four coupled PDEs; in §3 we apply linear stability analysis to the model, to determine the parameter regimes in which we can expect to observe aggregation, whilst in §4, we consider behaviour for long times. This is followed in §5 by numerical simulations of the governing equations. (A weakly nonlinear analysis of a modified version of the model is presented in Appendix A.) The paper concludes with a discussion in §6, summarising our main results, and suggesting possible directions for future work.

2 Model formulation

We consider an *in vitro* population of cells (hepatocytes) bathed in culture medium, which we treat as a two-phase mixture. The cells adhere to a deformable layer of ECM which occupies the base of the culture well (see Fig. 2). For simplicity, a one-dimensional slab geometry is adopted, we neglect the effects of chemotaxis and assume that the cells are nutrient-rich. The model is then developed, in §2.1, as a series of mass and momentum balances for the cells, culture medium and ECM. We close the model in §2.2 by introducing appropriate constitutive laws for the mechanical properties of each of the three species. Finally interaction forces and suitable boundary and initial conditions are specified in §2.3.

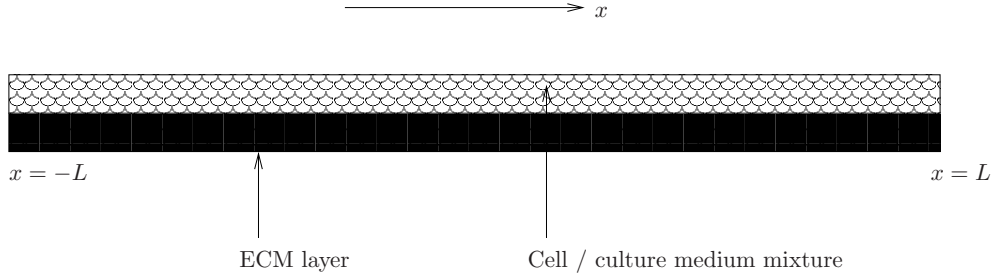


Figure 2: Definition sketch

2.1 Governing equations

We assume the culture well occupies the region $-L \leq x \leq L$. We denote the local volume fractions of the cells and culture medium by $n(x, t)$ and $w(x, t)$ and their horizontal velocities by $v_n(x, t)$ and $v_w(x, t)$. The ECM density and displacement are denoted by $\rho(x, t)$ and $s(x, t)$ respectively. For simplicity, we consider only small ECM displacements, so that linear theory is valid, and the ECM velocity is given by $\partial s / \partial t$.

In the cell and culture medium mixture we assume there are no voids, so

$$n + w = 1. \quad (1)$$

As cells consist predominantly of water, we assume that cells and culture medium have an equal, constant density ($\equiv 1$, without loss of generality) and exclude this factor from the relevant mass balance equations. Data on the rates of proliferation and death of hepatocytes in culture are limited. Enat et al. (1984) report that the ratio of the number of cells on day 7 of culture compared to that on day 1 is 1.0-2.9 (depending on the type of ECM and culture medium used), whilst Thomas et al. (2006) found around 10 % of cells died between 24 and 48 hours in culture. Since the timescale of interest for aggregation is around 1 day, this suggests that cell proliferation is not the main cause of cluster formation. For simplicity, we thus neglect hepatocyte proliferation and death, and likewise production and degradation of ECM, and hence obtain the following mass conservation equations for n, w and ρ :

$$\frac{\partial n}{\partial t} + \frac{\partial}{\partial x}(n v_n) = 0, \quad (2a)$$

$$\frac{\partial w}{\partial t} + \frac{\partial}{\partial x}(w v_w) = 0, \quad (2b)$$

$$\frac{\partial \rho}{\partial t} + \frac{\partial}{\partial x} \left(\rho \frac{\partial s}{\partial t} \right) = 0. \quad (2c)$$

We denote by σ_n, σ_w and σ_ρ the Cauchy stresses in the cells, culture medium and ECM. Neglecting inertial effects, the momentum balance in each phase is given by:

$$\frac{\partial}{\partial x}(n\sigma_n) + F_n = 0, \quad (3a)$$

$$\frac{\partial}{\partial x}(w\sigma_w) + F_w = 0, \quad (3b)$$

$$\frac{\partial \sigma_\rho}{\partial x} + F_\rho = 0, \quad (3c)$$

where F_n, F_w and F_ρ represent the net sources of momentum in each phase, the precise forms of which are discussed in §2.2.

2.2 Constitutive relations

We model the culture medium as an inviscid fluid for which

$$\sigma_w = -p, \quad (4)$$

where p is the fluid pressure.

We model the cells as an incompressible viscous fluid, with constant viscosity μ_n . The viscous effects are intended to capture the tendency of cells to align and match their velocities with the local average cell velocity (Babak et al., 2004). In the context of liver cell aggregation, the viscous term represents migration of hepatocytes as coupled pairs or groups (Powers and Griffith-Cima, 1996). Obviously, cells differ from viscous fluids in that they are able to generate forces in response to cues from their environment, such as variations in the local cell density. We assume these forces manifest themselves in the cellular phase as an additional pressure term, Σ_n . Thus, following Beward et al. (2002), we write

$$\sigma_n = -p - \Sigma_n + 2\mu_n \frac{\partial v_n}{\partial x}, \quad (5)$$

where

$$\Sigma_n = \Gamma_1 \frac{(n - n^*)}{(1 - n)^2}. \quad (6)$$

In the above, the tension constant, Γ_1 , describes the cells' affinity for the *close-packing* volume fraction $n^* \in (0, 1)$. We note from equation (3a) that it is in fact $n\Sigma_n$ that is key for cell movement. This function has a single turning point at $n = n_c = n^*/(2 - n^*)$. For $n < n_c$ the effect is for cells to move up gradients of n (*i.e.* cell-cell interactions are attractive), and conversely for $n > n_c$. A graph of $n\Sigma_n(n)$ is presented in Fig. 3.

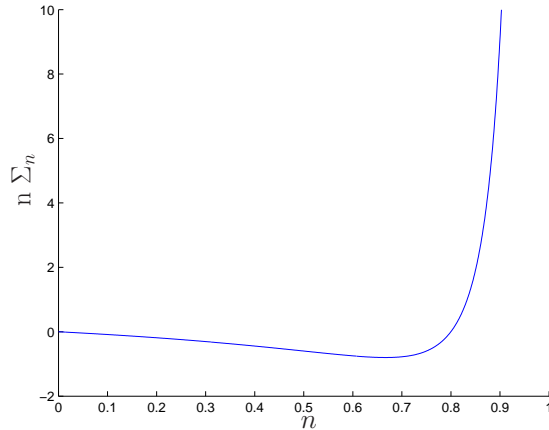


Figure 3: $n\Sigma_n$ against n ($n^*=0.8$, $\Gamma_1 = 1$).

We model the ECM as an isotropic, viscoelastic material, over which the cells move (see Fig. 2). In general, mechanochemical models are sensitive to the particular constitutive laws adopted (Byrne and Chaplain, 1996). However, in the absence of appropriate experimental data, we use the Voigt model of viscoelasticity (see e.g. Gracheva and Othmer, 2004) to describe the mechanical properties of the ECM. This model exhibits viscous behaviour over short timescales, and elastic behaviour at long times. The stress and displacement in the ECM are related as follows:

$$\sigma_\rho = \frac{\partial}{\partial x} \left(\mu_E \frac{\partial s}{\partial t} + E' s \right), \quad (7)$$

where μ_E and E' are the viscous and elastic constants for the material. (In fact, μ_E is the sum of the bulk and shear viscosities of the material, and E' is related to the Young's modulus E and Poisson ratio ν by $E' = E(1 - 2\nu)(1 - \nu)/(1 + \nu)$ (Murray, 1993).)

Turning to the momentum source terms, F_n , F_w and F_ρ , we assume that the culture medium and ECM exert drag forces on the cells (and *vice versa*), but neglect any drag between the ECM and the culture medium. Our choice of cell-ECM interaction term thus differs from that of Murray (1993), where a ‘tethering’ force proportional to the ECM displacement, s , is used. We denote by k_{nw} and $k_{n\rho}$ the cell-culture medium and cell-ECM drag coefficients and, following Breward et al. (2002), we fix $k_{nw} = k_1 n w$ and $k_{n\rho} = k_2 n \rho$ for non-negative constants k_1 and k_2 . Consequently there is no drag if either of the two species concerned is not present.

Combining the above information we write

$$F_n = -k_2 n \rho \left(v_n - \frac{\partial s}{\partial t} \right) - k_1 n w (v_n - v_w) + p \frac{\partial n}{\partial x}, \quad (8a)$$

$$F_w = -k_1 n w (v_w - v_n) + p \frac{\partial w}{\partial x}, \quad (8b)$$

$$F_p = k_2 n \rho \left(v_n - \frac{\partial s}{\partial t} \right). \quad (8c)$$

The last term in equations (8a) and (8b) represents the contribution of interfacial forces, assuming surface tension effects are negligible (see Drew and Segel (1971); Drew (1983) for a detailed derivation).

2.3 Initial and boundary conditions

The model comprises equations (2)-(3), together with the constitutive relations (4)-(8). We close the model by specifying appropriate boundary and initial conditions. The initial distribution of cells is given by

$$n(x, 0) = n_0(x). \quad (9)$$

Initially the ECM layer is taken to be undeformed and spatially uniform with constant density ρ_0 , so that

$$\rho(x, 0) = \rho_0, \quad s(x, 0) = 0. \quad (10)$$

We assume that the system is symmetric about $x = 0$; accordingly, we restrict attention to $0 \leq x \leq L$ and impose

$$s(0, t) = v_n(0, t) = v_w(0, t) = 0. \quad (11)$$

The ECM is taken to be pinned at the edge of the culture well, so the displacement is zero at $x = L$ - *i.e.*

$$s(L, t) = 0. \quad (12)$$

We also assume there is no flux of cells or water out of the culture well, so

$$v_n(L, t) = v_w(L, t) = 0. \quad (13)$$

2.4 Model simplification

The model developed in §§2.1 – 2.3 can be reduced to coupled PDEs for n , ρ , v_n and s . This allows us to focus on the four physical quantities with which we are most concerned. Although we eliminate the variables w , v_w and p , these quantities may be determined, if required, using expressions derived below.

Adopting the functional forms introduced in §2.2, the momentum balance equations (3) become:

$$\frac{\partial}{\partial x} \left(2\mu_n n \frac{\partial v_n}{\partial x} - n \Sigma_n \right) - n \frac{\partial p}{\partial x} - k_2 n \rho \left(v_n - \frac{\partial s}{\partial t} \right) - k_1 n w (v_n - v_w) = 0, \quad (14a)$$

$$w \frac{\partial p}{\partial x} + k_1 n w (v_w - v_n) = 0, \quad (14b)$$

$$\frac{\partial^2}{\partial x^2} \left(\mu_E \frac{\partial s}{\partial t} + E' s \right) + k_2 n \rho \left(v_n - \frac{\partial s}{\partial t} \right) = 0. \quad (14c)$$

Summing equations (2) leads to the incompressibility relation:

$$\frac{\partial}{\partial x} (n v_n + w v_w) = 0, \quad (15)$$

which, following integration and imposition of (11) yields:

$$v_w = \frac{-n v_n}{w} \quad (16)$$

(assuming $w \neq 0$). We combine equations (1) and (16) to eliminate w and v_w in (14b) and deduce that:

$$\frac{\partial p}{\partial x} = \frac{k_1 n}{(1-n)} v_n. \quad (17)$$

Using (17) in equation (14a) gives:

$$\frac{k_1 n}{(1-n)} v_n + k_2 n \rho \left(v_n - \frac{\partial s}{\partial t} \right) + \frac{\partial}{\partial x} (n \Sigma_n) - 2\mu_n \frac{\partial}{\partial x} \left(n \frac{\partial v_n}{\partial x} \right) = 0. \quad (18)$$

The reduced model comprises equations (2a), (2c), (14c) and (18) for n , ρ , s and v_n respectively, together with the initial and boundary conditions specified by equations (9)-(10), (11)-(13).

2.5 Parameters

Here we estimate the physical parameters in the model. The associated lengthscales range from the diameter of a cell ($\sim 10\mu\text{m}$) to that of a liver cell spheroid ($\lambda \sim 150\mu\text{m}$) to that

Parameter	Symbol	Units	Value	Source
Aggregate lengthscale	λ	m	10^{-4}	Thomas et al. (2005)
Domain half-length	L	m	10^{-2}	measured
Cell close-packing volume fraction	n^*	none	0.8	Powers et al. (2002)
Aggregation timescale	T^*	s	10^5	Riccalton-Banks (2002)
ECM density	ρ_0	kg m^{-3}	0.5-8	Namy et al. (2004) and refs. therein
Cell-water drag ^a	k_1	$\text{kg m}^{-3} \text{s}^{-1}$	10^7 - 10^{11}	Swabb et al. (1974); Lubkin and Jackson (2002)
Cell-ECM drag	k_2	$\text{kg m}^{-3} \text{s}^{-1}$	no data	N/A
Tension constant	Γ_1	$\text{kg m}^{-1} \text{s}^{-2}$	no data	N/A
Cell viscosity ^b	μ_n	s^{-1}	10^4 - 10^6	Forgacs et al. (1998); Lubkin and Jackson (2002)
ECM viscosity (collagen)	μ_E	$\text{kg m}^{-1} \text{s}^{-1}$	10^5	Velegol and Lanni (2001)
ECM shear modulus (collagen)	E'	Pa	10^0 - 10^1	Velegol and Lanni (2001)
ECM viscosity (PLA)	μ_E	$\text{kg m}^{-1} \text{s}^{-1}$	10^5 - 10^8	Namy et al. (2004); Chen et al. (2003); Gunatillake and Adhikari (2003)
ECM shear modulus (PLA)	E'	Pa	10^6 - 10^9	Namy et al. (2004); Chen et al. (2003); Gunatillake and Adhikari (2003)

^a measurements in (Swabb et al., 1974) relate to hepatoma.

^b measurements in (Forgacs et al., 1998) are for spherical aggregates of embryonic chick liver cells

Table 1: Summary of dimensional parameter values and the corresponding references

of the culture well ($L \sim 1\text{cm}$). Our interest in aggregation prompts us to use λ to fix a typical lengthscale. Our timescale T^* is related to the time for aggregation to occur ($T^* \sim 1$ day, (Riccaltan-Banks, 2002; Thomas et al., 2005)). We estimate the packing density to be $n^* = 0.8$ (see Powers et al. (2002))

The types of ECM used in liver tissue engineering include collagen gels and polylactic acid (PLA); for the former, $\mu_E \sim 10^5 \text{ Pa}$ and $E' \sim 10^0 - 10^1 \text{ Pa}$ (Velegol and Lanni, 2001), whilst for the latter, $\mu_E \sim 10^5 - 10^8 \text{ Pa}$ and $E' \sim 10^6 - 10^9 \text{ Pa}$ (Chen et al., 2003; Gunatillake and Adhikari, 2003; Namy et al., 2004). We thus consider a range of values for these parameters. The values of the cell viscosity μ_n , cell-culture medium drag constant k_1 and the initial ECM density ρ_0 are estimated from similar experiments reported in the literature. The parameter values and supporting references are summarised in Table 1.

At present, values for the cell-ECM drag constant, k_2 , and the tension constant Γ_1 cannot be determined from the literature and so must be estimated. We assume that the drag force between the cells and ECM is stronger than that between the cells and culture medium and hence take $k_2\rho_0 \geq k_1$. We estimate the timescale for aggregation in the absence of drag effects to be $T^* \sim 2\mu_n/\Gamma_1$, and use this to estimate Γ_1 . Given $T^* \sim 10^5 \text{ s}$ and using the range for μ_n stated in Table 1, we predict $\Gamma_1 \sim 10^{-1} - 10^1 \text{ kg m}^{-1} \text{ s}^{-2}$.

2.6 Dimensionless governing equations

We nondimensionalise as follows

$$\tilde{x} = \frac{x}{\lambda}, \quad \tilde{t} = \frac{\Gamma_1 t}{2\mu_n}, \quad \tilde{\rho} = \frac{\rho}{\rho_0}, \quad \tilde{v}_n = \frac{2\mu_n v_n}{\Gamma_1 \lambda}, \quad \tilde{s} = \frac{\mu_E s}{2\lambda\mu_n},$$

where tildes denote dimensionless quantities. Note that in the above, we have adopted the timescale $T^* = 2\mu_n/\Gamma_1$, which gives a balance between the cell viscosity and cell-generated forces. The dimensionless governing equations are then (dropping tildes for convenience):

$$\frac{\partial n}{\partial t} + \frac{\partial}{\partial x}(nv_n) = 0, \quad (19)$$

$$\frac{\partial \rho}{\partial t} + \frac{1}{\hat{\mu}} \frac{\partial}{\partial x} \left(\rho \frac{\partial s}{\partial t} \right) = 0, \quad (20)$$

$$\frac{\hat{k}_1 n}{(1-n)} v_n + \hat{k}_2 n \rho \left(v_n - \frac{1}{\hat{\mu}} \frac{\partial s}{\partial t} \right) + \frac{\partial}{\partial x} \left(\frac{n(n-n^*)}{(1-n)^2} \right) - \frac{\partial}{\partial x} \left(n \frac{\partial v_n}{\partial x} \right) = 0, \quad (21)$$

$$-\hat{k}_2 n \rho \left(v_n - \frac{1}{\hat{\mu}} \frac{\partial s}{\partial t} \right) = \frac{\partial^2}{\partial x^2} \left(\frac{\partial s}{\partial t} + \tau s \right), \quad (22)$$

where:

$$\hat{k}_1 = \frac{k_1 \lambda^2}{2\mu_n}, \quad \hat{k}_2 = \frac{k_2 \lambda^2 \rho_0}{2\mu_n}, \quad \hat{\mu} = \frac{\mu_E}{2\mu_n}, \quad \tau = \frac{2\mu_n E'}{\mu_E \Gamma_1}, \quad \epsilon = \frac{\lambda}{L}.$$

The parameters \hat{k}_1 and \hat{k}_2 are the ratios of cell-culture medium and cell-ECM drag to viscous forces; $\hat{\mu}$ is the ratio of the ECM and cell viscosities; and τ is the ratio of the aggregation timescale to the ECM relaxation time, $T_R = \mu_E/E'$ (*i.e.* T_R is the time taken for an ECM deformation to decay by a factor e^{-1} in the absence of external forces).

The initial conditions are now applied over the large domain $[0, \epsilon^{-1}]$ (given the length-scales stated in §2.5, $\epsilon^{-1} \approx 50$). They give

$$n(x, 0) = n_0(x), \quad \rho(x, 0) = 1, \quad s(x, 0) = 0, \quad (23)$$

whilst the boundary conditions for v_n and s become

$$v_n(0, t) = v_n(\epsilon^{-1}, t) = 0, \quad s(0, t) = s(\epsilon^{-1}, t) = 0. \quad (24)$$

3 Linear stability analysis

Equations (19)-(22), together with their associated boundary conditions (24) have a spatially homogeneous steady state solution for which $(n, \rho, v_n, s) = (n_0, 1, 0, 0)$ with $0 < n_0 < 1$ constant. This solution approximates the conditions immediately after the liver cells have been seeded in the culture wells. We examine the linear stability of this steady state to determine parameter ranges in which aggregation may occur. We consider perturbations of the form

$$n = n_0 + \hat{n}e^{iqx+\omega t}, \quad \rho = 1 + \hat{\rho}e^{iqx+\omega t}, \quad v_n = \hat{v}_n e^{iqx+\omega t}, \quad s = \hat{s}e^{iqx+\omega t}, \quad (25)$$

where the real part is to be understood, and $|\hat{n}|$, $|\hat{\rho}|$, $|\hat{v}_n|$ and $|\hat{s}| \ll 1$. Here, q is the wavenumber of a given perturbation and $\omega = \omega(q)$ is the corresponding growth rate. The no-flux boundary conditions impose the constraint $q = m\pi\epsilon$, where m is an integer.

For a given q , if there exists an $\omega(q)$ for which $\mathcal{R}(\omega) > 0$ (< 0), then the steady state is linearly unstable (stable) with respect to perturbations of the form (25). We expect aggregation to occur in parameter regimes for which the steady state is linearly unstable.

We substitute (25) into equations (19)-(22), linearise, and obtain the following dispersion relation for $\omega(q)$:

$$A(q^2)\omega^2 + B(q^2)\omega + C(q^2) = 0, \quad (26)$$

where

$$\begin{aligned} A &= \hat{k}_2 n_0 \left(\frac{\hat{k}_1}{(1-n_0)} + q^2 \right) + q^2 \hat{\mu} \left(\frac{\hat{k}_1}{(1-n_0)} + \hat{k}_2 + q^2 \right), \\ B &= q^2 \hat{\mu} \tau \left(\frac{\hat{k}_1}{(1-n_0)} + \hat{k}_2 + q^2 \right) + q^2 \beta(n_0) \frac{(\hat{k}_2 n_0 + q^2 \hat{\mu})}{(1-n_0)^3}, \\ C &= \frac{q^4 \tau \hat{\mu} \beta(n_0)}{(1-n_0)^3}, \end{aligned}$$

and $\beta(n_0) = 2n_0 - n^*(1+n_0)$. With the exception of $\beta(n_0)$, all model parameters are positive. Hence, $A > 0$ and the behaviour of (26) depends, via $\beta(n_0)$, on the signs of B and C . If $\beta(n_0) > 0$ then $B, C > 0$ and the system is linearly stable ($\mathcal{R}(\omega(q)) < 0$). If $\beta(n_0) < 0$ then $C < 0$ and the system is unstable (the roots of (26) are real and of opposite sign).

The above analysis suggests that the stability of the system depends only on the initial cell seeding density, n_0 . In particular, if $n_0 > n_c = n^*/(2-n^*)$ then $\beta(n_0) > 0$, the cell-cell interaction force is repulsive and the spatially uniform steady state is locally stable. If instead $n_0 < n_c$ then $\beta(n_0) < 0$ and the steady state is unstable, the cells moving to achieve their preferred density. We note from equation (26) that ω is bounded (but may be positive) as $q \rightarrow \infty$, since the highest power of q is the same in A , B and C . As a result modes with large wavenumber grow at almost equal rates. In order to distinguish between these modes the impact of nonlinear effects must be investigated. We use numerical methods to do this in §5, and illustrate how analytical methods may be used in Appendix A, where we perform a weakly nonlinear analysis of a modified version of the model. First, however, we consider the long-time dynamics.

4 Long-time behaviour

We consider the long-time behaviour of the model, by adopting the timescale $t = \delta^{-1}T$ (where $\delta \ll 1$). This has the effect of eliminating the time derivative term in equation (19) at leading order, and upon integrating and applying the boundary conditions, we find $nv_n = 0$. At leading order equation (22) then becomes:

$$\frac{\partial^2 s}{\partial x^2} = 0.$$

On integrating and applying the boundary conditions we find $s = 0$, and thus equation (20) (which is unchanged by the rescaling at leading order) implies ρ is an arbitrary function

of x (which will depend on the behaviour at earlier times). Assuming $n \neq 0$ (otherwise equation (21) is trivially satisfied), we find at leading order:

$$\frac{\partial}{\partial x} \left(\frac{n(n - n^*)}{(1 - n)^2} \right) = 0. \quad (27)$$

We observe that two types of behaviour may satisfy (27). The first possibility is that $n = \text{const.}$, but as we have seen from §3, the spatially uniform state is unstable for $n < n_c$, so we would not expect to observe this behaviour if at any time $n < n_c$ anywhere in the domain. The second possibility is that n is piecewise constant, taking the values 0 and n^* in different regions. This suggests that at long times, we may tend towards a situation in which there are aggregates within which the cells achieve their close-packing density, alternating with regions devoid of cells.

Since the role of cell-ECM adhesion is of particular interest, we also briefly consider the long-time behaviour in the limit of large \hat{k}_2 , for which cell-ECM drag is strong. Taking $\hat{k}_2 \gg 1$, we introduce the long timescale $t = \hat{k}_2 T$ and the slow cell velocity scale $v_n = V/\hat{k}_2$. Under these rescalings, equations (19) and (20) are unchanged at leading order, whilst equations (21) and (22) become

$$n\rho \left(V - \frac{\partial s}{\partial T} \right) + \frac{\partial}{\partial x} \left(\frac{n(n - n^*)}{(1 - n)^2} \right) = 0, \quad (28)$$

$$-n\rho \left(V - \frac{\partial s}{\partial T} \right) = \hat{\mu}\tau \frac{\partial^2 s}{\partial x^2}. \quad (29)$$

Combining equations (28) and (29) gives the following nonlinear diffusion equation for n

$$\frac{\partial n}{\partial T} + \frac{\partial}{\partial x} \left(n \frac{\partial s}{\partial t} - \frac{1}{\rho} \frac{\partial}{\partial x} \left(\frac{n(n - n^*)}{(1 - n)^2} \right) \right) = 0. \quad (30)$$

We note from (28) that V includes a term representing advection of the cells with the ECM as it is deformed. The form of this term is identical to that prescribed by Murray (1993), though we have derived it here from a momentum balance. We also note that equation (30) is ill-posed when $n < n_c = n^*/(2 - n^*)$; this would suggest the formation of localised regions of high or low cell density (Oliver et al., 2005). This is indeed what is seen numerically, with the formation of smaller aggregates for larger \hat{k}_2 (see *e.g.* Fig. 7). (We remark that, although the above equation is ill-posed, retention of a small viscous term in the full system renders it well-posed.)

The type of solution described in this section, in which the value of n changes abruptly in space, is similar to those involving the formation of shocks described in Byrne and

Preziosi (2003) for a two-phase model of tumour growth (in which the cell viscosity is neglected). Whilst the above analysis provides useful qualitative information on the long-time behaviour of our model, it does not tell us the positions at which n ‘jumps’, and hence the number of aggregates we can expect to observe. This will depend on the initial conditions, and the evolution of the model over $O(1)$ timescales, and must hence be investigated numerically. This is undertaken in the following section.

5 Numerical simulations

5.1 Numerical methods

The governing equations (19)-(22) were discretised using second-order accurate finite difference methods, and simulations were performed using MATLAB as follows. Firstly, given the initial conditions for n , ρ and s , we solved the discretised versions of equations (21) and (22) by a simple matrix inversion to obtain v_n and $\partial s/\partial t$. These values were then used to update n and ρ at the next timestep, using equations (19) and (20). The latter two equations are solved using a Crank-Nicholson type method (Strikwerda, 1989) (with the relevant velocities evaluated at the current timestep). We found it convenient to include a small stabilising diffusion term in equation (19) (with diffusion coefficient $D = 10^{-4}$) to reduce the number of points in the spatial discretisation needed to obtain satisfactorily smooth solutions. The solution for s was then updated using the values of $\partial s/\partial t$ found in the initial step, using a method which is first-order accurate in time. The updated solutions for n , ρ and s were then used to determine v_n and $\partial s/\partial t$ at the new timestep, and the process described above was repeated until the desired end time was reached. The growth rates of the numerical solutions for early times were verified against those predicted by the linear stability analysis.

For convenience, the domain is truncated to $0 \leq x \leq 10$ (numerical experiments with longer domains give the same qualitative results; results not presented). For the simulations presented in the following section, a timestep $\Delta t = 0.01$ and $N = 2001$ grid points were used.

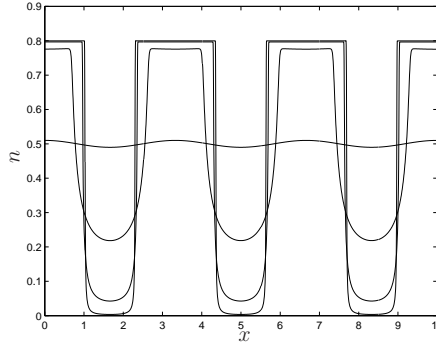


Figure 4: Numerical solution for cell volume fraction, n , at times $t = 0, 5, 10, 15$ ($\hat{k}_1 = \hat{k}_2 = \hat{\mu} = \tau = 1$).

5.2 Numerical results

Unless otherwise stated, henceforth we fix $n^* = 0.8$ and $\hat{k}_1 = \hat{k}_2 = \tau = \hat{\mu} = 1$, which is consistent with the ranges suggested in §2.5. For simplicity, we begin by setting $n(x, 0) = 0.5 + 0.01 \cos 0.6\pi x$ (other initial conditions will be considered later). The corresponding numerical simulations show the formation of aggregates which have sharply defined edges (except for those where the edge of the aggregate coincides with the edge of the domain), and uniform cell density (equal to $n^* = 0.8$) on the interior (Fig. 4). This agrees with the predictions of the long-time behaviour in §4. Note that in this simulation, the number of aggregates corresponds to the number of peaks in the initial condition.

During the early stages of aggregation, cell movement is slow (in Fig. 5 $|v_n| < 0.05$ for $0 \leq t \leq 2$). Between $t = 2$ and $t = 4$, the cell velocity increases considerably and aggregation proceeds relatively quickly (Fig. 5a). For $t \geq 5$, we note that we tend to observe $v_n = 0$ within aggregates (compare Figs. 4 and 5b); elsewhere $v_n \neq 0$, with the few remaining cells moving towards the nearest cluster. As the cells begin to aggregate, the ECM is at first pulled along with them, so that its density is increased within the growing aggregates (Fig. 6a). At later times, when most of the cells have stopped moving, elastic forces begin to reduce the deformation of the ECM (Fig. 6b) until its density becomes spatially uniform once again.

We now investigate the effect of varying key model parameters on the behaviour of the system. The parameters over which tissue engineers have most control are: the strength

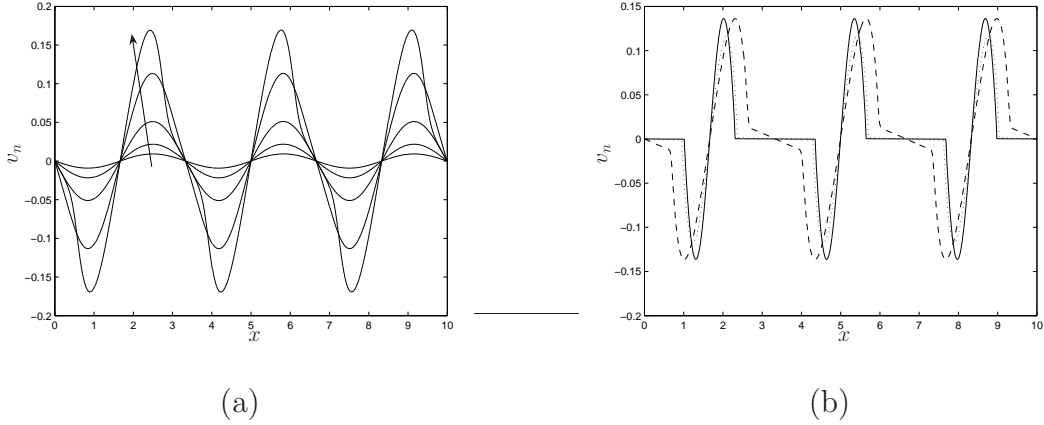


Figure 5: Numerical solution for cell velocity, v_n at: (a) $t = 0, 1, 2, 3, 4$ (arrow indicates increasing time); (b) $t = 5$ (dashed), $t = 10$ (dotted) and $t = 15$ (solid). Parameter values as for Fig. 4.

of cell-ECM adhesion \hat{k}_2 , which can be changed, for example, by surface modification of the substrate with various proteins; the physical properties of the ECM, represented by $\hat{\mu}$ and τ ; the degree of drag between the cells and the culture medium \hat{k}_1 , which will depend on the viscosity of the culture medium; and the initial cell seeding density, $n(x, 0)$.

Increasing the cell-ECM drag parameter \hat{k}_2 has two effects on cell aggregation. It increases the number of aggregates formed (with a corresponding reduction in their size) and reduces the cells' speed. Taking the same initial condition as for Fig. 4, and setting $\hat{k}_2 = 10$ (with other parameters unchanged), we see that initially, four aggregates begin to form as before. However, at later times, additional aggregates begin to form in the spaces between the original ones (Fig. 7a). By $t = 20$, 7 aggregates have formed (Fig. 7b). A further increase to $\hat{k}_2 = 30$ produces a further increase in the number of aggregates, to 9. In each case, there is a corresponding reduction in $|v_n|$ (results not presented). A similar effect occurs when the cell-culture medium drag parameter \hat{k}_1 is increased. Setting $\hat{k}_1 = 5$ (with other parameter values and initial conditions as for Fig. 4) results in the formation of 7 aggregates; whilst for $\hat{k}_1 = 10$ this number increases to 9 (results not presented).

Repeated simulations suggest that altering the ECM compliance (by changing $\hat{\mu}$ and τ) does not affect the qualitative nature of the cells' aggregation (results not presented). We do, however, see predictable changes in the ECM, with density variations almost eliminated for stiff substrates (large $\hat{\mu}$, τ) and increased deformation with increased compliance.

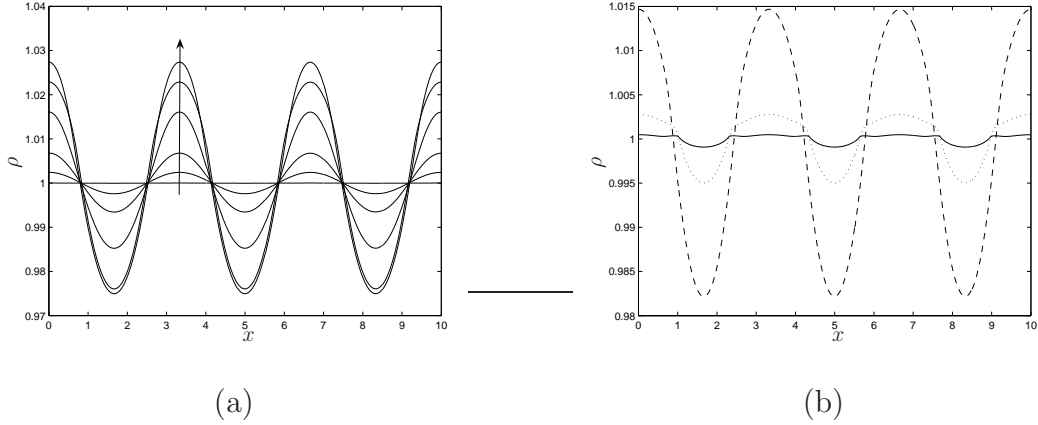


Figure 6: (a) Numerical solution for ECM density, ρ , at $t = 0, 1, 2, 3, 4, 5$ (arrow indicates increasing time) (b) $t = 6$ (dashed), $t = 10$ (dotted) and $t = 15$ (solid). Parameter values as for Fig. 4.

The final factor we wish to consider is the effect of the initial cell seeding density, $n(x, 0)$, on the formation of aggregates. We begin by setting the parameter values as for Fig. 4, and re-running the simulation for the initial condition $n(x, 0) = 0.6 + 0.01 \cos 0.6\pi x$. The result is that the same number of aggregates are formed as before, but the aggregates are larger, as there are more cells in the system (results not shown). If we continue to increase the cell seeding density, so that the initial condition has $n(x, 0) > n_c = 2/3$ (for $n^* = 0.8$), then the cells spread so that n becomes spatially uniform, as predicted by the linear stability analysis in §3. Still using the same parameter values, but with $n(x, 0) = 0.3 + 0.01 \cos 0.6\pi x$, we find that seven, rather than four, aggregates form (Fig. 8). The additional aggregates (which form between the four peaks of the initial condition) are extremely narrow.

A further question of interest is: how does the initial distribution of the cells affect the final number and size of aggregates? Our previous simulations, using sinusoidal initial conditions, impose a degree of symmetry on the solution which is unrealistic (though using these initial conditions is useful in identifying the effects of changing parameter values). In order to determine if the system dynamics naturally favour the formation of aggregates of a particular size, we considered the effect of using random initial conditions. These were obtained by taking the Fourier transform of a vector of length N , the entries of which were uniformly distributed on the interval $[0, 1]$. The higher-wavenumber ($q > 20$) modes were

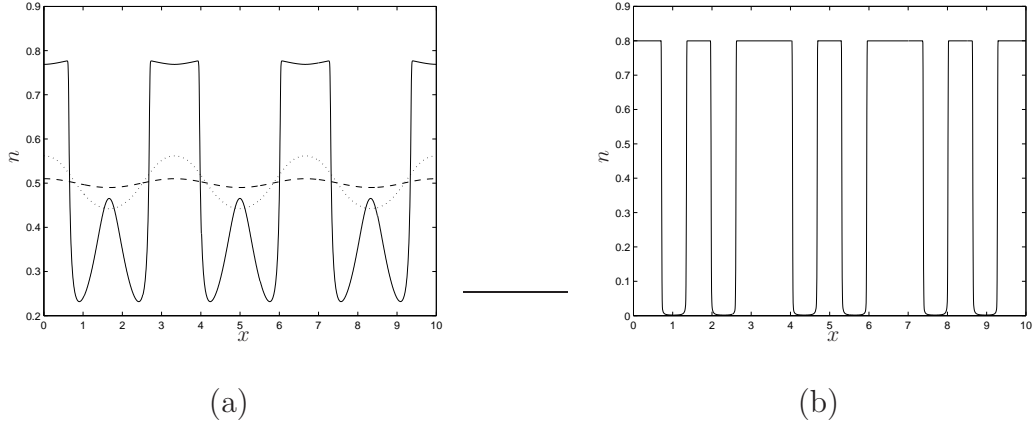


Figure 7: (a) Numerical solution for cell volume fraction, n , at $t = 0$ (dashed), $t = 5$ (dotted) and $t = 10$ (solid) (b) $t = 20$. Parameter values as for Fig. 4, except $\hat{k}_2 = 10$.

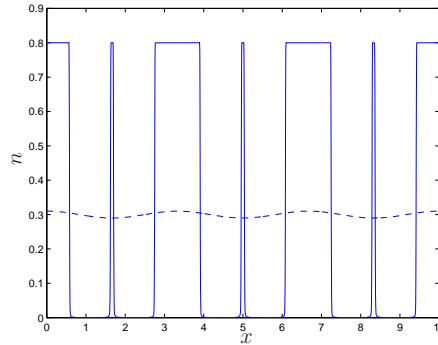


Figure 8: Numerical solution for n at $t = 0$ (dotted) and $t = 20$ (solid). Reduced cell seeding density $n(x, 0) = 0.3 + 0.01 \cos 0.6\pi x$. Parameter values as for Fig. 4.

then eliminated, and the inverse transform of the real part of the resulting vector was then normalised to give a perturbation with amplitude 0.01. We then set $n(x, 0) = \text{const.} + f(x)$, where $f(x)$ is the perturbation obtained as just described. Taking the parameter values as for Fig. 4, with the constant part of the initial condition set at 0.5, we performed five simulations for different realisations of the initial conditions. These resulted in the formation of the following numbers of aggregates: 7 (twice), 9 (twice), 11 (once). The average lengths of the aggregates (defined as regions where $n > 0.79$) were in the range 0.55 to 0.87. These results are broadly similar to those obtained with different random initial conditions, reported in (Green, 2006). This suggests that the initial conditions have only a limited influence on the number of aggregates that form.

6 Discussion

In this paper we have developed a new model of liver cell aggregation *in vitro*. The mass and momentum balances for the cell phase are similar to those of Kowalczyk et al. (2004), except that we neglect ‘inertia’ terms (which represent directional persistence). In addition, we have used a two-phase modelling framework to couple the motion of the cells and culture medium, postulating constitutive laws for the interaction forces between phases. Our simulations show the formation of ‘aggregates’ with clearly defined outer boundaries, and spatially uniform cell density in the interior. This is in good qualitative agreement with images of aggregates cultured *in vitro* (Riccalton-Banks et al., 2003; Thomas et al., 2005).

It is well known that both the strength of cell-ECM adhesion and the material properties of the ECM contribute significantly to cell mobility (Powers and Griffith-Cima, 1996; Thomas and DiMilla, 2000). Our results show that strong cell-ECM adhesion results in the formation of larger numbers of smaller aggregates, and increases the time taken for aggregates to form. Our results agree with experimental findings reported in Powers and Griffith-Cima (1996), that strong cell-substrate adhesion inhibits migration, and are consistent with the hypothesis that aggregates do not form when cell-ECM adhesions are stronger than cell contractile forces. When cell-ECM adhesion is extremely strong, we found cell movement was almost completely eliminated, which reproduces the experimental findings of Riccalton-Banks (2002) for cells seeded on tissue culture plastic. On the basis of these results we predict that reducing the strength of cell-substrate adhesion may promote the formation of large aggregates. In practice, some degree of cell-substrate adhesion may be necessary for cell locomotion, which would make the elimination of this effect undesirable.

In our model, the physical properties of the ECM (*i.e.* its viscosity and elastic modulus) do not have a significant effect on cell aggregation. However, this may be due to the assumption that the strength of cell-ECM adhesion (characterised by the parameter k_2) is independent of the ECM properties (characterised by μ_E and E'). Evidence already exists that some cell types form weaker adhesions to compliant substrates (Gracheva and Othmer, 2004), suggesting a more complex relation between the physical properties of the ECM and the strength of cell-ECM adhesion than has been assumed here. We could extend our model by replacing the parameter k_2 with a more complex function involving

μ_E and E' . However, although the current experimental literature contains a number of studies of spheroid formation on a variety of substrates, the mechanical properties of the substrates are not well characterised. We would suggest that further experimental investigation of the impact of the material properties of the substrate on cell adhesion may prove fruitful, and might allow us to postulate the form of a function to replace k_2 . Furthermore, our use of a drag term to model cell adhesion is also an idealisation of the biological situation. An alternative approach has been taken by Preziosi and Astanin (2005), who, when modelling the formation of capillaries, distinguished between a ‘viscous’ cell-ECM interaction force (equivalent to our cell-ECM drag term) and an ‘elastic’ force, which acts if the cells have had sufficient time to anchor to the ECM (or alternatively, if cells are moving sufficiently slowly), and is proportional to their relative displacement. We also remark that cell motility may depend on ECM properties, as a recent model of cell crawling (Thomas and DiMilla, 2000) suggests that cells move with maximum speed on rigid substrates: on compliant materials the ECM may deform preferentially relative to the cell, retarding cell motion. We could incorporate this effect by making the function Σ_n dependent upon ρ and the ECM’s mechanical properties.

Our simulations and analytical work suggest that the cell seeding density plays an important role in aggregate formation. In section §3, we showed that if the cells are seeded too densely (*i.e.* $n > n_c$), then aggregation will not occur. Our numerical results also suggest that reducing the cell seeding density leads to the formation of smaller aggregates. This agrees with experimental results reported by Tong et al. (1994). This, taken together with the findings above, suggests that the most favourable conditions for the formation of large-scale aggregates are high (but not too high) cell seeding density, and low cell-ECM and cell-culture medium drag.

The most obvious weakness of our model is the *ad hoc* adoption of a one-dimensional geometry. Furthermore, although we have not considered chemical signalling explicitly, aggregation is almost certainly influenced by chemical factors. For example, when hepatocyte conditioned medium (culture medium in which hepatocytes have previously been grown) is added to freshly isolated cells, their rate of aggregation increases (Fujii et al., 2000). This suggests that the hepatocytes produce a chemical signal which enhances their motility. Moreover, hepatocytes are known to respond chemotactically to hepatocyte growth factor (HGF) and epidermal growth factor (EGF) *in vitro* (Stolz and Michalopou-

los, 1997). Extending our model to investigate the impact of chemical signalling on cell aggregation would require us to augment our system of equations with an expression describing the production and diffusion of the chemical species and incorporate dependence upon the chemical concentration into the function Σ_n (Byrne and Owen, 2004). As a first step towards addressing these points, a two-dimensional version of the model (representing a vertical slice through the culture well), which also includes chemotaxis, has been developed by Green (2006). Thin-film approximations are then used to obtain one-dimensional systems of governing equations in two scaling regimes.

Alternatively, by extending our model to allow for multiple cell populations, we could investigate the impact of cellular heterogeneity on the rate of aggregation and the size of aggregates formed. Recent experimental research has looked at the effect of co-culturing hepatocytes with other cell types, such as hepatic stellate cells (Riccaltan-Banks et al., 2003), fibroblasts (Bhandari et al., 1997) and pancreatic islet cells (Lee et al., 2004). Under such conditions, spheroids appear to form more quickly, and may also be larger than those which arise in hepatocyte-only cultures. These cell types could easily be included as an additional phase within our multiphase framework.

In conclusion, this paper represents a first attempt to use mathematics to gain insights into the dynamics of spheroid formation, and our model predictions show good qualitative agreement with independent experimental results. In the absence of relevant experimental data, we were forced to make several modelling assumptions concerning, in particular, the nature of cell-substrate interactions and the constitutive law which describes the cells. Whilst we believe the form chosen for Σ_n is consistent with the type of interactions required to form aggregates of bounded cell density, other choices with the same qualitative behaviour (*i.e.* that the function is unbounded and positive as $n \rightarrow 1$, and has only one stationary point and one zero) might equally well have been considered. Extensions to the model, and careful validation against experimental results will be needed if our predictions are to be made quantitatively accurate. However, an advantage of our general model framework is that it can easily be extended or modified to take into account more complex experimental situations, as described above.

Acknowledgements

We would like to thank Dr Rena Bhandari and Mr Robert Thomas for helpful discussions, and Dr Lisa Riccalton-Banks for providing Fig.1. We are also grateful to Dr Andrew Grief and Dr James Oliver for assistance with the numerical simulations. JEFG was supported by a BBSRC studentship and SLW, KMS and HMB by EPSRC Advanced Fellowships.

References

- S. F. Abu-Absi, J. R. Friend, L. K. Hansen, and W. S. Hu. Structural polarity and functional bile canaliculi in rat hepatocyte spheroids. *Exp. Cell Res.*, 274:56–67, 2002.
- P. Babak, K. G. Magnusson, and S. Sigurdsson. Dynamics of group formation in collective motion of organisms. *Math. Med. Biol.*, 21:269–292, 2004.
- P. Bedossa and V. Paradis. Liver extracellular matrix in health and disease. *J. Pathol.*, 200:504–515, 2003.
- R. N. Bhandari, L. A. Riccalton, A. L. Lewis, J. R. Fry, A. H. Hammond, S. J. B. Tendler, and K. M. Shakesheff. Liver tissue engineering: A role for co-culture systems in modifying hepatocyte function and viability. *Tissue Eng.*, 7:345–357, 1997.
- C. J. W. Breward, H. M. Byrne, and C. E. Lewis. The role of cell-cell interactions in a two-phase model for avascular tumour growth. *J. Math. Biol.*, 45 (2):125–152, 2002.
- H. M. Byrne and M. A. J. Chaplain. The importance of constitutive equations in mechanochemical models of pattern formation. *Appl. Math. Lett.*, 9 (6):85–90, 1996.
- H. M. Byrne and M. R. Owen. A new interpretation of the Keller-Segel model based on multiphase modelling. *J. Math. Biol.*, 49(6):604–626, 2004.
- H. M. Byrne and L. Preziosi. Modelling solid tumour growth using the theory of mixtures. *Math. Med. Biol.*, 20:341–366, 2003.
- Centers for Disease Control and Prevention, 2003. Compressed Mortality File (CDC WONDER On-line Database - <http://wonder.cdc.gov>), Accessed 12 May 2003.
- C. Chen, J. Chueh, H. Tseng, H. Huang, and S. Lee. Preparation and characterisation of biodegradable PLA polymeric blends. *Biomaterials*, 24:1167–1173, 2003.

- D. A. Drew. Mathematical modelling of two-phase flow. *Ann. Rev. Fluid Mech.*, 15: 261–291, 1983.
- D. A. Drew and L. A. Segel. Averaged equations for two-phase flows. *Stud. Appl. Math.*, 3:205–231, 1971.
- R. Enat, D. M. Jefferson, N. Ruiz-Opazo, Z. Gatmaitian, L. A. Leinwand, and L. M. Reid. Hepatocyte proliferation *in vitro*: Its dependence on the use of serum-free hormonally defined medium and substrata of extracellular matrix. *Proc. Natl. Acad. Sci. USA*, 81: 1411–1415, 1984.
- G. Forgacs, R. A. Foty, Y. Shafrir, and M. S. Steinberg. Viscoelastic properties of living embryonic tissues: a quantitative study. *Biophys. J.*, 74:2227–2234, 1998.
- Y. Fujii, K. Nakazawa, and K. Funatsu. Intensive promotion of spheroid formation by soluble factors in a hepatocyte-conditioned medium. *J. Biomater. Sci. Polym. Ed.*, 11 (7):731–745, 2000.
- R. Glicklis, L. Shapiro, R. Agbaria, J. C. Merchuk, and S. Cohen. Hepatocyte behaviour within three-dimensional porous alginate scaffolds. *Biotechnology and Bioengineering*, 67(3):344–353, 2000.
- R. Glicklis, J. C. Merchuk, and S. Cohen. Modelling mass transfer in hepatocyte spheroids via cell viability, spheroid size and hepatocellular functions. *Biotechnology and Bioengineering*, 86(6):672–680, 2004.
- M. E. Gracheva and H. G. Othmer. A continuum model of motility in ameboid cells. *Bull. Math. Biol.*, 66:167–193, 2004.
- J. E. F. Green. *Mathematical modelling of cell aggregation in liver tissue engineering*. PhD thesis, University of Nottingham, UK, 2006.
- P. A. Gunatillake and R. Adhikari. Biodegradable synthetic polymers for tissue engineering. *Eur. Cell. Mater.*, 5:1–16, 2003.
- A. Higuchi and Y. Tsukamoto. Cell separation of hepatocytes and fibroblasts through surface-modified polyurethane membranes. *Journal of Biomedical Materials Research Part A*, 71A(3):470–479, 2004.

- T. L. Jackson and H. M. Byrne. A mechanical model of tumour encapsulation and transcapsular spread. *Math. Biosci.*, 180:307–328, 2002.
- H. O. Jauregui. *Principles of Tissue Engineering (Second Edition)*, chapter 39 : Liver, pages 541–551. Academic Press, 2000.
- E. F. Keller and L. A. Segel. Initiation of slime mold aggregation viewed as an instability. *J. Theor. Biol.*, 26:399–415, 1970.
- E. F. Keller and L. A. Segel. Model for chemotaxis. *J. Theor. Biol.*, 30:225–234, 1971.
- R. Kowalczyk, A. Gamba, and L. Preziosi. On the stability of homogeneous solutions to some aggregation models. *Discrete and Continuous Dynamical Systems: B*, 4(1):203–220, 2004.
- K. W. Lee, S. K. Lee, J. W. Joh, S. J. Kim, B. B. Lee, K. W. Kim, and K. U. Lee. Influence of pancreatic islets on spheroid formation and functions of hepatocytes in hepatocyte-pancreatic islet spheroid culture. *Tissue Eng.*, 10:965–77, 2004.
- G. Lemon, J. R. King, H. M. Byrne, O. E. Jensen, and K. M. Shakesheff. Mathematical modelling of engineered tissue growth using a multiphase porous flow mixture theory. *J. Math. Biol.*, 52:571–594, 2006.
- S. R. Lubkin and T. Jackson. Multiphase mechanics of capsule formation in tumours. *J. Biomech. Eng.*, 124:237–243, 2002.
- P.K. Maini and J. D. Murray. A nonlinear analysis of a mechanical model for biological pattern formation. *SIAM J. Appl. Math.*, 48(5):1064–1072, 1988.
- P. C. Matthews and S. M. Cox. Pattern formation with a conservation law. *Nonlinearity*, 13(4):1293–1320, 2000.
- T. Mitaka. The current status of primary hepatocyte culture. *Int. J. Exp. Pathol.*, 79:393–409, 1998.
- P. V. Moghe, F. Berthiaume, R. M. Ezzell, M. Toner, R. G. Tompkins, and M. L. Yarmush. Culture matrix configuration and composition in the maintenance of hepatocyte polarity and function. *Biomaterials*, 17:373–385, 1996.

- P. V. Moghe, R. N. Cogger, M. Toner, and M. L. Yarmush. Cell-cell interactions are essential for maintenance of hepatocyte function in collagen gel but not on matrigel. *Biotechnol. Bioeng.*, 56 (6):706–710, 1997.
- J. D. Murray. *Mathematical Biology*. Springer-Verlag, New York, 2nd edition, 1993.
- P. Namy, J. Ohayon, and P. Tracqui. Critical conditions for pattern formation and *in vitro* tubulogenesis driven by cellular traction fields. *J. Theor. Biol.*, 227:103–120, 2004.
- NHS, 2001. Liver activity. UK transplant activity 2001, UK Transplant - NHS, 2001.
- J. M. Oliver, J. R. King, K. J. McKinlay, D. M. Grant, C. A. Scotchford, J. V. Wood, and P. D. Brown. Thin film theories for two-phase reactive flow models of active cell motion. *Math. Med. Biol.*, 22:53–98, 2005.
- OPTN, 2003. Donors and waiting list 1993-2003. Organ Procurement and Transplantation Network (www.optn.org), Accessed 16 Sept. 2003.
- M. R. Owen, H. M. Byrne, and C. E. Lewis. Mathematical modelling of the use of macrophages as vehicles for drug-delivery to hypoxic tumour sites. *J. Theor. Biol.*, 226:377–391, 2004.
- M. V. Peshwa, F. J. Wu, B. D. Follstad, F. B. Cerra, and W. Hu. Kinetics of hepatocyte spheroid formation. *Biotechnol. Prog.*, 10:460–466, 1994.
- M. V. Peshwa, F. J. Wu, H. L. Sharp, F. B. Cerra, and W. Hu. Mechanistics of formation and ultrastructural evaluation of hepatocyte spheroids. *In Vitro Cell Dev. Biol.*, 32:197–203, 1996.
- M. J. Powers and L. Griffith-Cima. Motility behaviour of hepatocytes on extracellular matrix substrata during aggregation. *Biotechnology and Bioengineering*, 50:392–403, 1996.
- M. J. Powers, R. E. Rodriguez, and L. G. Griffith. Cell-substratum adhesion strength as a determinant of hepatocyte aggregate morphology. *Biotechnology and Bioengineering*, 53:415–426, 1997.
- M. J. Powers, K. Domansky, M. R. Kaazempur-Mofrad, A. Kalezi, A. Capitano, A. Upadhyaya, P. Kurzawski, K. E. Wacka, D. B. Stolz, R. Kamm, and L. G. Griffith. A

- microfabricated array bioreactor for perfused 3D liver culture. *Biotechnol. Bioeng.*, 78(3):257–269, 2002.
- L. Preziosi and S. Astanin. Modelling the formation of capillaries. In A. Quarteroni, editor, *Integration of Complex Systems in Biomedicine*, chapter 4. Springer, 2005.
- L. Riccalton-Banks, C. Liew, R. Bhandari, J. Fry, and K. Shakesheff. Long-term culture of functional liver tissue: Three-dimensional coculture of primary hepatocytes and stellate cells. *Tissue Eng.*, 9(3):401–409, 2003.
- L. A. Riccalton-Banks. *Maintenance of Primary Rat Hepatocytes in vitro Using Co-culture Techniques*. PhD thesis, University of Nottingham, 2002.
- L. Richert, D. Binda, G. Hamilton, C. Viollon-Abadie, E. Alexandre, D. Bigot-Lasserre, R. Bars, P. Coassolo, and E. LeCluyse. Evaluation of the effect of culture configuration on morphology, survival time, antioxidant status and metabolic capacities of cultured rat hepatocytes. *Toxicol. In Vitro*, 16:89–99, 2002.
- C. Selden, M. Khalil, and H. J. F. Hodgson. What keeps hepatocytes on the straight and narrow? Maintaining differentiated liver function. *Gut*, 44:443–446, 1999.
- D. B. Stolz and G. K. Michalopoulos. Synergistic enhancement of EGF, but not HGF, stimulated hepatocyte motility by TGF- β 1 *in vitro*. *J. Cell. Physiol.*, 170:57–68, 1997.
- J. C. Strikwerda. *Finite difference schemes and partial differential equations*. Wadsworth and Brooks / Cole Advanced Books and Software, Belmont, California, USA, 1989.
- E. A. Swabb, J. Wei, and P. M. Gullino. Diffusion and convection in normal and neoplastic tissues. *Cancer Res.*, 34:2814–2822, 1974.
- R. J. Thomas, R. Bhandari, D. A. Barrett, A. J. Bennett, J. R. Fry, D. Powe, B. J. Thomson, and K. M. Shakesheff. The effect of three-dimensional co-culture of hepatocytes and hepatic stellate cells on key hepatocyte functions *in vitro*. *Cells Tissues Organs*, 181:67–79, 2005.
- R. J. Thomas, A. Bennett, B. Thomson, and K. M. Shakesheff. Hepatic stellate cells on poly(DL-lactic acid) surfaces control the formation of 3D hepatocyte co-culture aggregates *in vitro*. *Euro. Cell. Mater.*, 11:16–26, 2006.

- T. W. Thomas and P. A. DiMilla. Spreading and motility of human glioblastoma cells on sheets of silicone rubber depend on substratum compliance. *Med. Biol. Eng. Comput.*, 38:360–370, 2000.
- J. Z. Tong, S. Sarrazin, D. Cassio, F. Gauthier, and F. Alvarez. Application of spheroid culture to human hepatocytes and maintenance of their differentiation. *Biology of the Cell*, 81:77–81, 1994.
- B. Vasiev and C. J. Weijer. Modelling of *Dictyostelium discoideum* slug migration. *J. Theor. Biol.*, 223:347–359, 2003.
- D. Velegol and F. Lanni. Cell traction forces on soft biomaterials. I Microrheology of type I collagen gels. *Biophys. J.*, 81:1786–1792, 2001.
- M.J. Whitaker. *Supercritical Fluid Processing of Polymers, Proteins and Cells for Tissue Engineering Applications*. PhD thesis, University of Nottingham, 2003.

A Weakly nonlinear analysis

In this appendix, we undertake a weakly nonlinear analysis (Maini and Murray, 1988) of the 1D model developed in §2.1, and construct approximate solutions to the governing equations when the system is close to marginal stability. To perform this analysis, we introduce an additional diffusion term (with coefficient D) on the RHS of equation (19) which stabilises the highest wavenumber modes; without it, standard techniques cannot be applied, as there are an infinite number of unstable modes. (We justify the inclusion of a diffusion term on the basis that it describes more realistically the behaviour of the cells, which will undergo a small amount of random motion, and that it replicates the numerical method used in §5.) We focus on the limit $\hat{k}_2 = 0$ in which cell-ECM adhesion is negligible, as this simplifies the analysis considerably. The equations under consideration are thus

$$\frac{\partial n}{\partial t} + \frac{\partial}{\partial x} (nv_n) = D \frac{\partial^2 n}{\partial x^2}, \quad (31)$$

$$\kappa(n)v_n + \frac{\partial}{\partial x} (n\Sigma_n(n)) - \frac{\partial}{\partial x} \left(n \frac{\partial v_n}{\partial x} \right) = 0. \quad (32)$$

In (32), we have left the additional pressure term Σ_n in general form, and introduced $\kappa(n)$ as a general form of the cell-culture medium drag term. (For the choice of drag coefficient

specified in §2.2, we would have $\kappa(n) = \hat{k}_1 n / (1 - n)$.) We solve (31)-(32) subject to the boundary conditions:

$$v_n = 0, \quad \frac{\partial n}{\partial x} = 0 \quad \text{at } x = 0, \frac{1}{\epsilon}. \quad (33)$$

We now repeat the linear stability analysis of §3 for equations (31) and (32). We consider small-amplitude perturbations to the spatially homogeneous steady state of the form:

$$n = n_0 + \hat{n}e^{iqx + \omega t}, \quad v_n = \hat{v}_n e^{iqx + \omega t}, \quad (34)$$

where q and ω are, respectively, the wavenumber and growth rate of the perturbation and $|\hat{n}|, |\hat{v}_n| \ll 1$. Substituting (34) into equations (31) and (32) yields:

$$\omega = -q^2 \left(D + \frac{n_0 \Lambda'(n_0)}{(\kappa(n_0) + n_0 q^2)} \right), \quad (35)$$

where $\Lambda(n) = n \Sigma_n$ and a prime denotes differentiation. We hence note that, for instability to occur, we require:

$$\Lambda'(n_0) < \frac{-D(\kappa(n_0) + n_0 q^2)}{n_0}. \quad (36)$$

The addition of the diffusion term is stabilising, as we would expect, since in the limit $D \rightarrow 0$, we require $\Lambda'(n_0) < 0$ (or equivalently $\beta < 0$ in the notation of §3).

We note from (35) that if

$$D + \frac{n_0 \Lambda'(n_0)}{(\kappa(n_0) + n_0 q^2)} = 0, \quad (37)$$

then $\omega = 0$ (*i.e.* the growth rate is undetermined at leading order). Condition (37) can be viewed as specifying a critical wavenumber, q , given fixed values of n_0 and D . Alternatively (37) may be used to determine critical parameter values for which a given wavenumber q has $w(q) = 0$. We note further that in order to satisfy the boundary conditions at $x = 0, 1/\epsilon$, we require that the additional condition $q = m\pi\epsilon$ (where m is an integer) must hold. In fact, it is necessary to assume the stronger constraint $m = 1$, as for $m > 1$, there exists a smaller permissible wavenumber, for which $\mathcal{R}(\omega) > 0$. We would then expect this longer-wavelength mode to dominate.

To determine the growth rate, we rescale the governing equations on a longer timescale. We introduce a small parameter, $0 < \delta \ll 1$, and adopt a long timescale $t = \delta^{-2} T$. Equation (32) is unchanged as a result of this rescaling, whilst (31) becomes:

$$\delta^2 \frac{\partial n}{\partial T} + \frac{\partial}{\partial x} (n v_n) = D \frac{\partial^2 n}{\partial x^2}. \quad (38)$$

We seek solutions of the form:

$$n = n_0 + \delta n_1(x, T) + \delta^2 n_2(x, T) + \dots, \quad v_n = \delta v_1(x, T) + \delta^2 v_2(x, T) + \dots, \quad (39)$$

and also write $D = D_0 + \delta^2 D_1 + \dots$, where D_0 is the value of D satisfying (37) - *i.e.*

$$D_0 = -\frac{n_0 \Lambda'(n_0)}{(\kappa(n_0) + n_0 q^2)}. \quad (40)$$

At $O(\delta)$, equations (38) and (32) give:

$$n_0 \frac{\partial v_1}{\partial x} = D_0 \frac{\partial^2 n_1}{\partial x^2}, \quad (41)$$

$$n_0 \frac{\partial^2 v_1}{\partial x^2} = \left(\kappa(n_0) + \frac{n_0 \Lambda'}{D_0} \right) v_1. \quad (42)$$

Solving the above subject to the boundary conditions yields, and using (37) gives

$$n_1 = -\left(\frac{n_0}{D_0 q} \right) A(T) \cos qx, \quad v_1 = A(T) \sin qx, \quad (43)$$

where $q = \pi \epsilon$ and $A(T)$ is the amplitude of velocity (which is also related to the amplitude of n_1), which is determined at $O(\delta^3)$.

Continuing to next order, we find:

$$n_0 \frac{\partial v_2}{\partial x} + \frac{\partial}{\partial x} (n_1 v_1) = D_0 \frac{\partial^2 n_2}{\partial x^2} \quad (44)$$

$$\kappa(n_0) v_2 + \kappa'(n_0) n_1 v_1 + \Lambda'(n_0) \frac{\partial n_2}{\partial x} + \Lambda''(n_0) n_1 \frac{\partial n_1}{\partial x} - n_0 \frac{\partial^2 v_2}{\partial x^2} - \frac{\partial}{\partial x} \left(n_1 \frac{\partial v_1}{\partial x} \right) = 0. \quad (45)$$

We seek solutions of the form:

$$n_2 = N_2 A^2(T) \cos(2qx), \quad v_2 = V_2 A^2(T) \sin(2qx), \quad (46)$$

where N_2 and V_2 are constants. Substituting these forms into equations (44) and (45) yields:

$$N_2 = \frac{n_0}{(2D_0 q)^2} \left[1 - \left(\frac{1}{3q^2} \left(\frac{\Lambda'(n_0)}{D_0} + \kappa'(n_0) \right) + \frac{2}{3} + \frac{n_0 \Lambda''(n_0)}{3D_0 q^2} \right) \right], \quad (47)$$

$$V_2 = \frac{1}{6D_0 q^3} \left(\kappa'(n_0) + \frac{\Lambda'(n_0)}{D_0} \right) + \frac{1}{3D_0 q} + \frac{n_0 \Lambda''(n_0)}{6D_0^2 q^3}. \quad (48)$$

At $O(\delta^3)$, we have:

$$\frac{\partial n_1}{\partial T} + \frac{\partial}{\partial x} (n_1 v_2 + n_2 v_1) + n_0 \frac{\partial v_3}{\partial x} = D_0 \frac{\partial^2 n_3}{\partial x^2} + D_1 \frac{\partial^2 n_1}{\partial x^2}, \quad (49)$$

$$\begin{aligned} \kappa(n_0)v_3 + \kappa'(n_0)(n_1v_2 + n_2v_1) + \frac{\kappa''(n_0)}{2}n_1^2v_1 + \Lambda'(n_0)\frac{\partial n_3}{\partial x} + \Lambda''(n_0)\frac{\partial}{\partial x}(n_1n_2) \\ + \frac{\Lambda'''(n_0)n_1^2}{2}\frac{\partial n_1}{\partial x} - n_0\frac{\partial^2 v_3}{\partial x^2} - \frac{\partial}{\partial x}\left(n_1\frac{\partial v_2}{\partial x} + n_2\frac{\partial v_1}{\partial x}\right) = 0. \end{aligned} \quad (50)$$

In order to suppress the resonant terms, we require:

$$\begin{aligned} -\frac{\kappa'(n_0)A^3}{2}\left(N_2 + \frac{n_0V_2}{D_0q}\right) + \frac{\kappa''(n_0)A^3}{8}\left(\frac{n_0}{D_0q}\right)^2 + \frac{q^2A^3}{2}\left(N_2 - \frac{2n_0V_2}{D_0q}\right) \\ - \frac{\Lambda'(n_0)}{D_0}\left[\left(\frac{n_0}{D_0q^2}\right)\left(\frac{dA}{dT} + q^2D_1A\right) + \frac{A^3}{2}\left(N_2 + \frac{n_0V_2}{D_0q}\right)\right] + \frac{q\Lambda''(n_0)N_2}{2}\left(\frac{n_0}{D_0q}\right)A^3 \\ + \frac{q\Lambda'''(n_0)}{8}\left(\frac{n_0}{D_0q}\right)^3A^3 = 0. \end{aligned} \quad (51)$$

The above hence reduces to the Landau equation (Maini and Murray, 1988)

$$\frac{dA}{dt} = \alpha_1A + \alpha_2A^3, \quad (52)$$

where the coefficients are given by:

$$\alpha_1 = -q^2D_1, \quad (53)$$

$$\begin{aligned} \alpha_2 = \frac{q^2D_0^2}{n_0\Lambda'(n_0)}\left[\frac{-\kappa'(n_0)}{2}\left(N_2 + \frac{n_0V_2}{D_0q}\right) + \frac{\kappa''(n_0)}{8}\left(\frac{n_0}{D_0q}\right)^2 + \frac{q^2}{2}\left(N_2 - \frac{2n_0V_2}{D_0q}\right) \right. \\ \left. - \frac{\Lambda'(n_0)}{2D_0}\left(N_2 + \frac{n_0V_2}{D_0q}\right) + \frac{q\Lambda''(n_0)N_2}{2}\left(\frac{n_0}{D_0q}\right) + \frac{q\Lambda'''(n_0)}{8}\left(\frac{n_0}{D_0q}\right)^3\right], \end{aligned} \quad (54)$$

and, D_0 is related to Λ' , q and κ by equation (40).

The long-time behaviour of the amplitude equation is thus:

(i) For $D_1 > 0$ and $\alpha_2 > 0$, $A \rightarrow 0$ if $A(0) < \sqrt{(|\alpha_1|/\alpha_2)}$; $A \rightarrow \infty$ if $A(0) > \sqrt{(|\alpha_1|/\alpha_2)}$.

(ii) For $\alpha_2 < 0 < D_1$, $A \rightarrow 0$.

(iii) For $D_1 < 0 < \alpha_2$, $A \rightarrow \infty$.

(iv) For $D_1 < 0$ and $\alpha_2 < 0$, $A \rightarrow \sqrt{(\alpha_1/|\alpha_2|)}$.

A sketch illustrating how the system dynamics vary in different regions of (D, n_0) parameter space is presented in Fig. 9, with $q = 0.1\pi$, $\kappa(n_0) = n_0/(1 - n_0)$ and $\Lambda(n_0) = n_0(n_0 - 0.8)/(1 - n_0)^2$ (these are equivalent to the dimensionless functions used in §2.6 with $\hat{k}_1 = 1$ and $n^* = 0.8$). The space is divided up by the curves $\alpha_1 = 0$ (*i.e.* $D = D_0$), and those across which $\alpha_2(n_0)$ changes sign; the latter are vertical lines occurring at $n_0 = n_\alpha \approx 0.5$ (corresponding to a root of $\alpha_2(n_0) = 0$) and $n_0 = n_c = 2/3$, where n_c is as defined in §3 (corresponding to a discontinuity across which α_2 changes sign, since

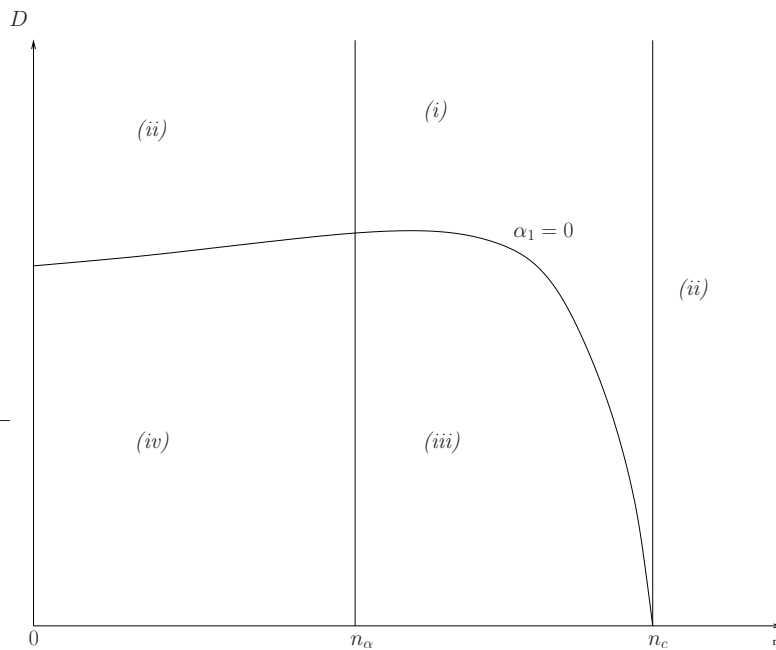


Figure 9: Behaviour of solutions in different regions of (D, n_0) parameter space (with $q = 0.1\pi$, $\kappa(n_0) = n_0/(1 - n_0)$ and $\Lambda(n_0) = n_0(n_0 - 0.8)/(1 - n_0)^2$). Labels (i) - (iv) refer to the regimes described in the main text. Note that n_α and n_c are the values of n_0 across which α_2 changes sign (see main text for details). For the given parameter values, $n_\alpha \approx 0.5$, and $n_c = 2/3$ (see §3).

$D_0(n_c) = \Lambda'(n_c) = 0$). The behaviour of α_2 is quite sensitive to the choice of n^* *e.g.* for $n^* = 0.9$, there is an additional root of $\alpha_2 = 0$ for $n < n_c$. (Note that owing to the assumption that $D = D_0 + \delta^2 D_1$, the predictions of the analysis are only valid for choices of D close to the $\alpha_1 = 0$ curve.)

Numerical simulations of the governing PDEs in the relevant region of parameter space confirms the predictions of the weakly nonlinear analysis (results not shown). The analysis presented above is valid for a finite interval and breaks down on an infinite domain. In this case, variation of the dependent variables on the long lengthscale (*i.e.* much longer than the critical wavelength) must be included, together with the potential for mode interaction (Matthews and Cox, 2000).